RESEARCH ARTICLE

Macromolecular Reaction Engineering
www.mre-journal.de

Fouling Pathways in Emulsion Polymerization Differentiated with a Quartz Crystal Microbalance (QCM) Integrated into the Reactor Wall

*Andreas Böttcher, Judith Petri, Arne Langhoff, Stephan Scholl, Wolfgang Augustin, Annika Hohlen, and Diethelm Johannsmann**

Emulsion polymerization fouling at hot interfaces is studied in situ, making use of a quartz crystal microbalance with dissipation monitoring (QCM-D). The resonator crystal is heated with a ring-shaped thermal pad from the back, turning it into a plate with elevated temperature. Configured to be one of the walls of a small reactor for emulsion polymerization, this resonator is prone to heat-transfer fouling, similar to regular heated parts of process equipment. The fouling kinetics is readily quantified with this QCM. During polymerization at constant temperature (80 °C), some deposition is always observed. However, a film with a thickness of less than 1 μm (determined gravimetrically with the QCM) is sometimes found, which stabilizes the surface against the deposition of much thicker layers. When reaction fouling proceeds directly to thick deposits, a small increase in resonance bandwidth often occurs a few minutes prior to the main transition, presumably caused by coagulum formed in the bulk making first contact with the surface. Furthermore, particle fouling is studied with temperature ramps on nonreactive dispersions. Fouling, if present, is readily observed.

1. Introduction

The unwanted deposition of solid material on the surfaces of process equipment such as reactors, heat exchangers, pipes, and tanks is a pervasive problem in the chemical industry and elsewhere. These "fouling" layers may be of nanoscopic thickness in membrane fouling,[1] but otherwise, fouling usually implies a thickness in the range of tens of micrometers and more. Adsorbates with a thickness of less than a micrometer by themselves are unproblematic as far as heat transfer and pressure drop are concerned. They are common and they do play a role in fouling, either by conditioning the surface for further fouling[2] or by passivating it.

In the chemical industry, fouling at hot interfaces (heat-transfer fouling) is particularly widespread.[2–4] An example is limescale in heat exchangers, that is, the irreversible formation of solid calcium carbonate, driven by the decreased solubility at high temperature.[5,6] Limescale lowers the efficiency of heat transfer across the respective interface and at the same time increases the pressure drop in the pipe. Heat-transfer fouling is also common in polymerization reactions, in which case, the fouling process is driven at least in part by chemical reactions at the hot wall. Fouling is among the reasons, why emulsion polymerization to date is mostly carried out as a batch process in industry.[7–10] Continuous processes have been demonstrated,[11] but suffer from the danger of clogging. Heat-transfer fouling is particularly severe in emulsion polymerization because latex dispersions are complex media with various mechanisms of destabilization.

The fouling mechanisms in emulsion polymerization are roughly classified as particle fouling[12] and reaction fouling.[13,14] Particle fouling can be caused by shear gradients at the wall, leading to orthokinetic destabilization.[12] It can also be the consequence of poor colloidal stability at elevated temperatures. Some protective colloids (surface-attached polymers, stabilizing the latex spheres against aggregation) show decreased solubility in water at high temperature, similar to the calcium salts in crystallization fouling. The decreased solubility is linked to the hydrophobic interaction between polymer chains. Being an entropically driven interaction, the hydrophobic interaction increases with increasing temperature. To be distinguished from particle fouling is reaction fouling.[13,15] Deposition of solid organic material at a hot wall may simply be the consequence of an increased polymerization rate. Particle fouling and reaction fouling can synergistically promote each other. This interplay was emphasized

A. Böttcher, J. Petri, A. Langhoff, D. Johannsmann
Institute of Physical Chemistry
Clausthal University of Technology
Arnold-Sommerfeld-Str. 4, 38678 Clausthal-Zellerfeld, Germany
E-mail: johannsmann@pc.tu-clausthal.de

S. Scholl, W. Augustin, A. Hohlen
Institute of Chemical and Thermal Process Engineering
Technische Universität Braunschweig
Langer Kamp 7, 38106 Braunschweig, Germany

The ORCID identification number(s) for the author(s) of this article can be found under https://doi.org/10.1002/mren.202100045

DOI: 10.1002/mren.202100045

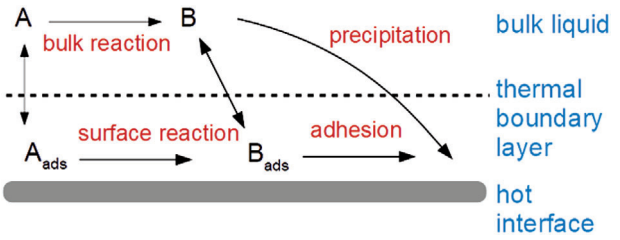

Figure 1. Pathways of reaction fouling following ref. [13]. Material may adsorb to the hot surface either before or after the reaction. In the former case, polymerization at the surface can be expected to proceed differently from the bulk. In the context of emulsion polymerization, "precipitation" is similar to particle fouling.

by Watkinson with a sketch reproduced in **Figure 1**.[13] In this diagram, reaction fouling in the narrow sense is shown as "$A \rightarrow A_{ads} \rightarrow B_{ads}$." The path "$A \rightarrow B \rightarrow B_{ads}$" (to be distinguished from precipitation) denotes reaction fouling in a wider sense.

Techniques to monitor and quantify heat-transfer fouling have been reviewed in ref. [16]. Two easily available parameters are the drop in pressure over the length of the tube and the efficiency of heat transfer. Pressure and temperature are routinely monitored in chemical lines, regardless of fouling. Thermal resistance is a well-suited fouling parameter whenever heat transfer is the main concern from an application point of view. For more detailed mechanistic studies, pressure and temperature as fowling indicators suffer from limited sensitivity. If the diagnostics is based on thermal resistance, the limit of detection is equivalent to a thickness of a few micrometers. The initial stages of fouling therefore are not seen. Also, there is no direct one-to-one relation between pressure and temperature, on the one hand, and fouling, on the other.

Ref. [16] describes electrical and acoustic techniques as alternatives. Fouling detection based on the layer's electrical impedance is possible, when the surface and the bulk are electrically conductive.[17] A similar method is exploited in electrochemical impedance spectroscopy[18] and in electrical cell-surface impedance spectroscopy.[19] High temperature (and variable temperature, in particular) interferes with these measurements because the electrical conductivity is temperature-dependent. Among the acoustic techniques is reflectometry.[20] Depending on the details, the amplitude and the phase of the reflected wave may report the layer's compressional-wave impedance (related to its softness) in addition to the layer thickness.[20] A second class of acoustic instruments makes use of vibrating surfaces integrated into the wall. These launch surface waves, traveling along the interface affected by fouling.[21] The speed of propagation and the damping are changed by the fouling layer. Excitation and detection occur with transducers outside the sensing area. The dynamic range can to some extent be adapted to the sample by choosing the frequency (and thereby the wavelength) accordingly. The quartz crystal microbalance (QCM) also amounts to a vibrating surface. It is discussed in more detail below.

2. The QCM as an Instrument to Detect and Quantify Fouling

The QCM consists of a thin piezoelectric plate, displaying acoustic thickness-shear resonances with frequencies in the megahertz range.[22] Deposition of some layer on the plate's surface lowers the resonance frequency, which turns the QCM into a rather simple and robust film thickness monitor. Under favorable conditions (constant temperature and bulk viscosity), the limit of detection can be well below 1 nm. The advanced QCMs (also termed "QCM-D" for QCM with dissipation monitoring) report the resonance bandwidth in addition to the resonance frequency and they do so on a number of different overtones.[23] This added information typically is turned into an estimate of the sample's softness.

Fouling detection with a QCM is straightforward, in principle. As of August 2021, the Web of Science returns 130 publications to the search term "QCM and fouling." (The search term "QCM and heat-transfer fouling" does not return any results). Many of the publications on the QCM applied to fouling problems are concerned with biofouling[24] and its prevention. Membrane fouling also plays a role. One publication targets latex dispersions (additives in paper making, in this case).[25] Ref. [26] reports on a study of the formation of limescale and the inhibition thereof by electrochemical means. Thick microbial biofilms have also been studied.[24,27] Ref. [28] addresses quality control in water treatment.

The QCM is very well suited to the study of fouling when, first, the temperature can be maintained constant, and when, second, the layer thickness is less than 500 nm. Constant temperature avoids the problems addressed in Section 3 (temperature–frequency coupling, temperature-dependent bulk viscosity). Thin films simplify the analysis. If the film thickness is much below the wavelength of shear sound, the QCM operates as a gravimetric device. The overtone-normalized frequency shifts, $\Delta f/n$ with n the overtone order, are the same on all overtones and they are proportional to the area-averaged layer thickness. The shift in half bandwidth, $\Delta\Gamma$, in this case- is smaller than the shift in frequency, which amounts to a test for whether or not the QCM actually operates in the gravimetric regime. If it does, small deviations from perfectly gravimetric behavior can be exploited to infer the layer's shear modulus (Section S IV, Supporting Information).

This type of analysis works less well when the layer thickness approaches a quarter of the wavelength of sound, $\lambda/4$. The wavelength of sound, λ, is a few micrometers, depending on the overtone order and the material's shear modulus. Because the viscoelastic effects then are large, they cannot always be separated from the gravimetric effects, and the derived values of the thickness are correspondingly uncertain. Also, area averaging is more problematic than in the thin-layer case. There is a side aspect to this problem. Around a thickness of $\lambda/4$, the QCM data go through a coupled resonance (also: "film resonance" in this particular geometry). The layer forms a resonator of its own, analogous to the vibrating reed in some musical instruments. The film resonance occurs when the wave's phase shift per round trip through the film equals 2π. When the film thickness is about $\lambda/4$, the wave acquires a phase of π while traveling though the film (back and forth). It acquires a second phase of π when it is reflected at the interface between the film and the resonator. The latter phase shift occurs because the shear-wave impedance of the resonator is much higher than the shear-wave impedance of the film. With a total phase shift of 2π, constructive interference results. The amplitude becomes large and the dissipated energy (proportional to the resonance bandwidth) goes through a maximum. The film resonance (more generally, any coupled

resonance) is linked to a characteristic feature in the QCM data. Frequency and bandwidth go through wiggles, which form circles or ellipses in polar diagrams (in plots of $\Delta\Gamma$ vs Δf). A quantitative analysis of such data in terms of thickness or shear modulus is difficult, but a coupled resonance as such is indicative of the sample being a film, as opposed to an assembly of flakes of coagulum. This argument will be important in Section 5.1.2.

A side remark on the parameter $\Delta\Gamma$: This work uses the half bandwidth (Γ) to quantify dissipative processes at the QCM surface. Also in use is the dissipation factor, $D = 2\Gamma/f_{res}$, and shifts thereof (ΔD in units of 10^{-6}). For 5 MHz resonators, ΔD and $\Delta\Gamma/n$ are related as $\Delta\Gamma/n = 2.5 \times (\Delta D/10^{-6})$ Hz.

The analysis again becomes easy, technically, when the layer thickness is much larger than the wavelength of sound. For viscous materials, the wavelength of sound and the penetration depth of the shear wave are of similar magnitude. The penetration depth of the shear wave is a few hundred nanometers in water and other low-viscosity liquids. It can be many micrometers in polymer films.[29] In view of the large decay length in sufficiently stiff films, the dynamic range of this QCM (the maximum quantifiable thickness of the fowling layer, in particular) can be many micrometers.

When the fouling layer is thick, when the material is soft, and when it covers the entire resonator surface, the QCM senses the material's shear modulus, rather than the thickness. The shear modulus may certainly be of interest. For instance, the modulus increases when the material becomes more compact. As noticed by Groves et al. in the context of coagulation dipping,[30] wet sintering and compactification usually are slower than the formation of the deposit (of natural rubber in this case, eventually forming rubber gloves). The same is true here, evidenced by the fact that the deposits are white. They contain voids, which act as scattering centers for light.

Again, the QCM in the latter limit does no longer report the amount of fouling material. This remark amounts to a caveat with regard to the interpretation of some of the experiments discussed at the beginning of this section. For thick, soft fouling layers, the frequency shift should not be naively converted to film thickness, because the Sauerbrey equation may or may not be applicable to these layers.

Acoustic devices capable of monitoring thicker films have been described.[31] A lowered resonance frequency (that is, a longer wavelength) is needed, which makes the QCM less sensitive at the low end and at the same time expands its dynamic range toward thicker films. These kilohertz resonators include the torsional resonators.[32]

3. Configuring the QCM as a Heat-Transfer Surface

Temperature effects are a well-known problem in the operation of the QCM. First, there is the intrinsic temperature–frequency coupling (*T*–*f* coupling). The "temperature-compensated cuts" (which include the AT cut) lead to small *T*–*f* coupling at room temperature (a few ppm K^{-1}), but only at room temperature. Worse, *T*–*f* coupling is hysteretic because it involves the migration of crystal defects. The resonator does not return to its original state after having been heated.

For experiments in air, *T*–*f* coupling only affects the frequency, not the resonance bandwidth. In liquids, though, bandwidth also

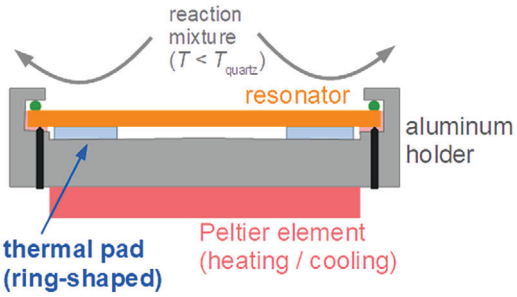

Figure 2. Sketch of the QCM setup. Central to this work is the possibility to heat a running resonator with a ring-shaped thermal pad, contacting the resonator from the back.

couples to temperature because the bandwidth depends on the viscosity of the bulk, following the Kanazawa–Gordon relation.[33] These effects may be accounted for with calibration, in principle, but this requires a precise knowledge of the temperature of the liquid close to the resonator surface. For fast-evolving situations as encountered in heat-transfer fouling, subtracting the bulk effects from the effects caused by a fouling layer is difficult. It is difficult even conceptually, when the fouling layer is thicker than the depth of penetration of the shear wave. The fouling layer then in effect takes the role of the bulk.

The difficulties with temperature acknowledged, temperature ramps have been exploited by others with considerable success. The experiments in ref. [34] were carried out in air. Hysteresis was seen, but was not detrimental. Possibly, one can fight hysteresis in fouling experiments (as observed here) by mounting the resonator more carefully. Among the sources of hysteresis is static stress. Static stress in temperature cycling may be particularly strong in this geometry, where the thermal pad touches the resonator from the back (**Figure 2**).

Usually, the temperature of a liquid-phase QCM is controlled from the side of the liquid. Being a thin plate (≈330 μm in thickness for a 5 MHz crystal), the resonator quickly adopts the temperature of the bulk. For the study of heat-transfer fouling, however, the resonator must be warmer than the liquid. It turns out that heating the resonator from the back is feasible with a ring-shaped thermal pad inserted into the cavity behind the resonator (**Figure 2**). Such a pad might have been expected to overdamp the resonance, but the resonator was found to operate perfectly well as long as the thermal pad contained a central hole with a large-enough diameter (≈8 mm, where the diameter of the resonator is 1 in.). Because the amplitude of oscillation is large in the center and decreases toward the edge, a compromise between good thermal contact, on the one hand, and limited acoustic damping, on the other, can be found. The constraints on acoustic damping are moderate because the resonator is also damped by the sample to a considerable degree. An estimate of the time constant for thermal equilibration can be obtained from the thermal conductivity and the specific heat capacity of crystalline quartz. The thermal diffusivity is $\lambda = \kappa/(\rho c_p)$ with κ the thermal conductivity, ρ the density, and c_p the specific heat capacity in units of J K^{-1} kg^{-1}. Inserting values, one finds λ to be about 8×10^{-7} m^2 s^{-1}. The time for equilibration is of the order of r^2/λ with $r = 4$ mm, the radius of the hole. Following this argument, the time needed for thermal equilibration is about 20 s. Experiment indicates that

this problem is not severe. Optical images of the resonator after experiments rarely show the center of the resonator to be free of a fouling layer, if the edge is not. The problem needs attention, though.

As shown in Section 5.1, the baseline stability at constant temperature over a duration of 1 h is better than the root-mean-square noise. The latter is 5 Hz (on a time base of 1 s), which amounts to a limit of detection (LOD) of 15 Hz (corresponding to 3 nm, following the Sauerbrey equation with $\rho = 1\ \mathrm{g\ cm^{-3}}$). The sensitivity of this QCM is in the nanometer range (depending on the averaging time). The LOD of this QCM is worse than the LOD achieved with room-temperature QCMs by about a factor of 100. Reasons are the large *T–f* coupling at high temperature, convection, and pressure fluctuations caused by stirring.

4. Experimental Section

The QCM is a home-built device. Annotated drawings are provided in the Supporting Information. The resonances were interrogated with impedance analysis. The vector network analyzer (VNA, supplied by Makarov Instruments, Toronto) was based on the N2PK design.[35] The resonators (diameter of 1 in., gold electrodes) were purchased from Quartz Pro, Stockholm. The QCM surface may be covered with functional layers of various kinds. Section 5.1.2 reports on experiments, in which the gold electrode was covered with a metallic layer mimicking stainless steel. Particle fouling (Section 5.2) was also tested with coatings of SiO_x and with spin-cast layers of polystyrene (data not shown).

Figure 3 shows the reaction chamber. The walls consisted of the resonator (to the left) and a bent glass cylinder, clamped to the holder of the resonator. The glass cylinder was not temperature-controlled in any way. Heating only occurred across the resonator and the aluminum structure holding it. The thermal pad was of the type Kerafol 86/300. Its thickness was 1 mm. The material's thermal conductivity is 3 $\mathrm{W\ m^{-1}\ K^{-1}}$. The resonator plate was mounted vertically, so that neither sedimentation nor creaming would drive coagulated material to the sensor surface. The stirrer was shaped as a propeller, creating a jet directed toward the resonator surface.

The nominal temperature was measured at the back of the holder. Given that the cell was only heated from the side, the temperature in the cell was less than the temperature of the holder. Figure S1 (Supporting Information) shows temperatures determined with a thermocouple immersed in the liquid close to the resonator surface. This thermocouple replaced the stirrer and therefore could not be installed while polymerizations were running. From Figure S1 (Supporting Information), one inferred that a nominal temperature of 80 °C corresponded to a temperature of about 65 °C in the liquid at a distance of about 1 mm from the surface. (Again, the temperature strongly varied in the cell because the cell was heated from the left, only.)

Polymerization was carried out as follows: deionized water, monomer (either butyl acrylate or methyl methacrylate, BA or MMA) were thoroughly stirred to produce small monomer droplets, and purged of oxygen by bubbling with nitrogen. In some cases, acrylic acid was used as a comonomer (10% of total monomer) to aid colloidal stability. Surfactant (5 mg) was added after purging with N_2. The surfactants were Dowfax 2A1 (anionic), Disponil FES77 (nonionic), or a 1:1 mixture of the two.

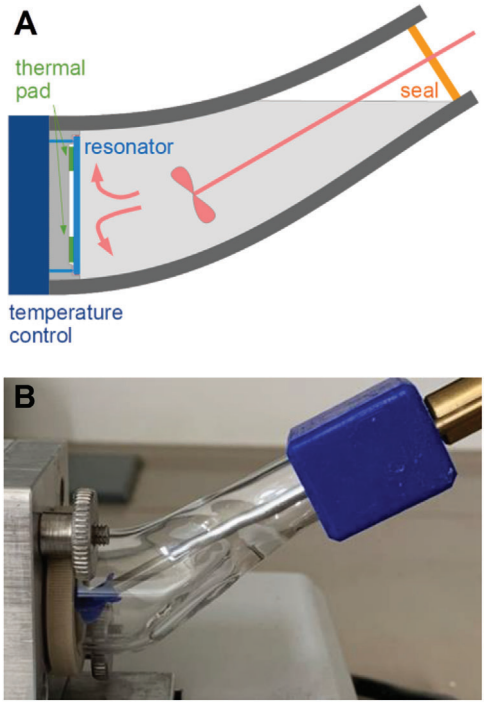

Figure 3. A,B) The reaction chamber (sketch in (A), photograph in (B)) has a volume of 14 mL. The dark gray line in (A) denotes a bent glass cylinder. Heating occurs from the resonator and its holder (to the left). The stirrer is shaped as a propeller, pumping the liquid toward the heated surface. For more detailed drawings, see the Supporting Information.

The total volume after addition of the initiator was 14 mL. The ratios of monomer to water were adjusted to achieve solid contents of 5%, 10%, or 30% w/w, as indicated in the graphs in Section 5. The reaction mixture was filled into the chamber and the chamber was heated to the desired nominal temperature of 80 °C. After a baseline was acquired, the polymerization was started by adding the initiator ($Na_2S_2O_8$, 0.1 g dissolved in 1 mL of water). As discussed in Section 5.1, the addition of initiator left a trace in the QCM data, namely small fluctuations in frequency, caused by small excursions in temperature. The reaction was allowed to proceed for about 2 h. QCM data were taken while the polymerization was running. At the end of the experiment, the reaction mixture became turbid. When the QCM indicated fouling, fouling was also evident in visual inspection after disassembly of the chamber.

Figure 4 shows data from a reference experiment with the thermal pad omitted. The process studied was supposed to be a polymerization at constant temperature, similar to the experiments shown in Section 5.1. Without the thermal pad, polymerization did not actually take place because the reaction mixture was hardly heated, at all. There still were small fluctuations in frequency and bandwidth, mostly caused by fluctuations in temperature. Neither polymerization (which would have been evidenced by turbidity) nor fouling took place.

Particle fouling (Section 5.2) was studied in separate experiments, where nonreactive dispersions were filled into the chamber and submitted to temperature ramps. These experiments suffered from hysteresis, but fouling (or the absence thereof) was

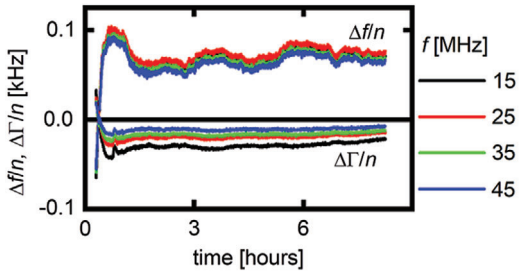

Figure 4. A reference experiment undertaken under the same conditions as the experiments discussed in Section 5.1, but with the thermal pad behind the resonator plate omitted. The resonator plate is not heated and emulsion polymerization does not take place. As expected, fouling does not occur, either. The reaction mixture was clear after the experiment (no polymer dispersion). The variations in frequency and bandwidth are caused by temperature fluctuations. They are unrelated to the formation of a deposit.

still seen and could be analyzed with regard to its kinetics. The quantitative analysis was more complicated than the analysis of experiments at constant temperature.

5. Results and Discussion

5.1. Reaction Fouling

5.1.1. Formation of Large Amounts of Fouling Material

Figure 5 shows results from experiments, which eventually produced thick deposits. QCM data were acquired in parallel to the polymerization reaction of BA (panels A–D) and MMA (panel E) at constant temperature. The panels on the right-hand side expand the data from the left to let the small step in $\Delta\Gamma/n$ occurring before the main step be visible more clearly. For BA, fouling produces a sharp increase in $\Delta\Gamma/n$ and $-\Delta f/n$. The magnitudes of $-\Delta f/n$ and $\Delta\Gamma/n$ are similar, indicative of a soft deposit with a thickness larger than the depth of penetration of the shear wave. The values saturate to levels between 1 and 4 kHz. Under conditions of saturation, the area-averaged thickness is larger than the penetration depth of the shear wave. The frequency shift then remains unchanged if further material is added to the top of the layer. The behavior of polymethyl methacrylate (PMMA) is similar to the behavior of polybutyl acrylate (PBA), but the transition is less sharp and the small step in $\Delta\Gamma$ a few minutes before the main transition is absent. Possibly, the difference goes back to PMMA being a glassy material, which does not undergo wet sintering[36] to the same degree as PBA.

For BA, the large step in the QCM data is always preceded by a smaller step. The small step is more pronounced in $\Delta\Gamma/n$ than in $-\Delta f/n$. Also, $\Delta\Gamma/n$ decreases with increasing overtone order, which amounts to $\Delta\Gamma$ being independent of overtone order. The canonical interpretation of such a finding is sketched in **Figure 6**. The complex frequency shift, $\Delta f + i\Delta\Gamma$, is proportional to the area-averaged complex amplitude of the stress exerted onto the resonator surface by the sample. The ratio of the shear stress to the transverse velocity is the "load impedance."[23] Impedances of this kind have analogies in electricity (in which case the impedance is a voltage-to-current ratio rather than a stress-to-velocity ratio). As in electricity, there are equivalent circuits available for modeling. While the assignment of

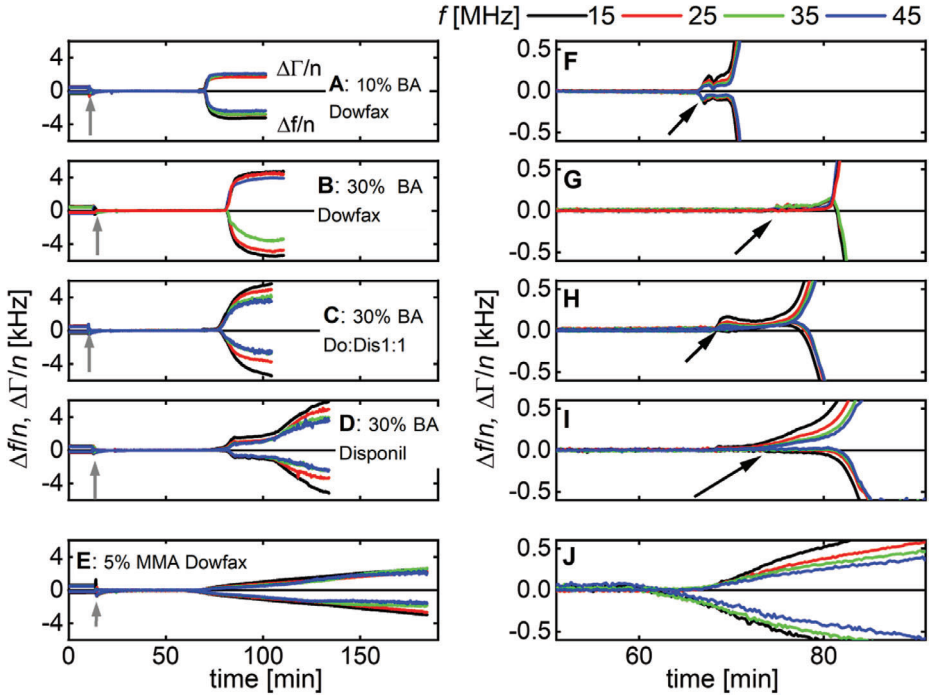

Figure 5. Overtone-normalized shifts of frequency and bandwidth acquired in parallel to emulsion polymerization of A–D) butyl acrylate (BA) or E) methyl methacrylate (MMA) at constant temperature. Percentages indicate the solids content. Gray vertical arrows in panels (A–E) denote the time, at which the initiator was added. F–J) Expanding the data from panels (A–E) to more clearly show the small, sudden increase in bandwidth a few minutes before the main transition (black arrows, only seen for BA). Presumably, this is the time of first contact with coagulum.

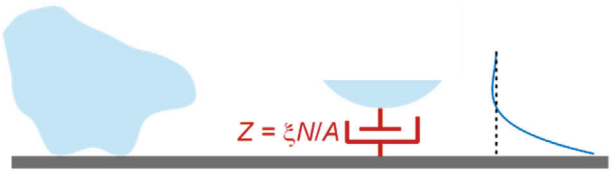

Figure 6. A shift in bandwidth, only, with $\Delta\Gamma$ independent of overtone order (as in Figure 5H) can be attributed to a dashpot. This behavior may be caused by narrow, soft links to large clusters. The geometrical configuration is depicted on the left. The center shows the mechanical equivalent circuit. The blue line to the right sketches the decaying shear wave. $\xi = F/v$ is the friction coefficient of the bridge, where F is the transverse force and v is the velocity of the substrate. Both F and v are complex amplitudes. N/A is the number density of adsorbed clusters. Z is the total load impedance generated by the ensemble of bridges.

experimental features to equivalent circuits is not unique, the simplest circuit, which predicts $\Delta\Gamma >> -\Delta f$ and $\Delta\Gamma$ independent of overtone order, is the dashpot. The dashpot is the mechanical equivalent of the resistor, which also dissipates energy and which lets the dissipated energy be independent of frequency. It is difficult to explain this behavior with other circuits and this behavior is not actually common in experiment. The left-hand side in Figure 6 depicts the experimental geometry, which corresponds to the dashpot. Large clusters of particles (flakes) contact the surface across small, soft, viscous bridges. The bridges must be narrower than the penetration depth of the shear wave in order to behave like a dashpot. The large clusters extend to beyond the penetration depth of the shear wave, so that they do not take part in the resonator's movement as a whole. In terms of the equivalent circuit, they constitute a rigid wall. The load impedance then is given as $\xi N/A$ with ξ the ratio of force to velocity of the dashpot (the friction coefficient), and N/A the number density of contacts. The progress of fouling within this picture is not an increase in thickness of some layer ("$A \leftrightarrow A_{ads} \rightarrow B_{ads}$" in Figure 1). It rather amounts to an increase in density of adsorbed clusters ("$A \rightarrow B \rightarrow B_{ads}$" in Figure 1). This is one of the cases where reaction fouling and particle fouling are not strictly separate. While the chemical reaction certainly promotes the fouling process, the coalescence of particles does play a role.

5.1.2. Formation of Thin Layers

In the experiments shown in **Figure 7**, the deposition of polymer on the resonator proceeded much differently. The samples from Figure 7 are films with a rather homogeneous thickness. The sample underlying Figure 7A consisted of PBA copolymerized with acrylic acid, which improves colloidal stability. The experiment underlying Figure 7B occurred with steel-covered electrodes.

These results from Figure 7 are in line with the Sauerbrey picture.[37] **Figure 8** emphasizes the fundamental difference between these two pathways of deposition in diagrammatic form. Thick deposits are to be distinguished from thin passivation layers.

In Figure 7, the overtone-normalized frequency shifts are similar on the different overtones and the shifts in bandwidth are smaller than the shifts in frequency. There is a maximum in

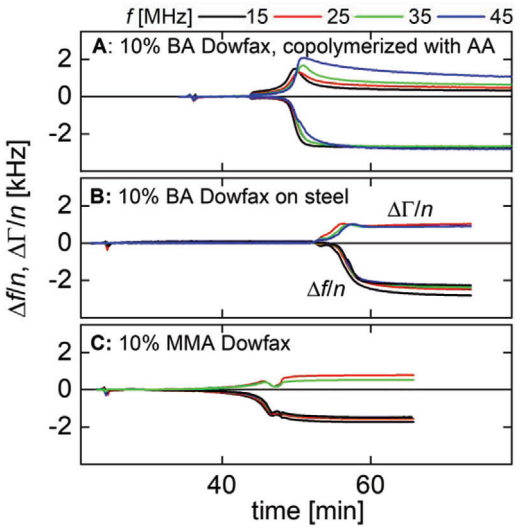

Figure 7. A–C) Experiments where deposition resulted in the formation of a thin film. The experimental conditions are indicated in the legends. Eventually, the shift in bandwidth, $\Delta\Gamma$, is smaller than the negative frequency shift, $-\Delta f$. Also, the overtone-normalized frequency shifts, $-\Delta f/n$, are similar between overtones. This behavior is characteristic of planar layers.

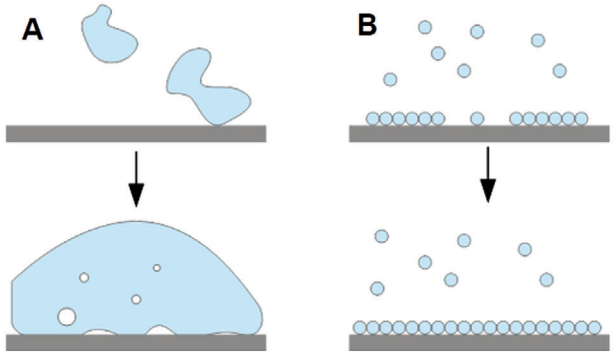

Figure 8. Sketch of the two separate pathways for fouling. A) Bulk-like fouling: the small increase in $\Delta\Gamma$ preceding the large decrease in Δf presumably is caused by the attachment of coagulum formed in the bulk, which later covers the entire surface and compactifies. B) Formation of thin films: the thin films evidenced by the data from Figure 7 are compatible in thickness with few layers of spheres. Presumably, these adsorb individually and prevent further fouling because they repel other spheres (similar to how different particles repel each other in the liquid dispersion).

bandwidth at intermediate times. In Figure 7C, the maximum in $\Delta\Gamma$ is accompanied by small wiggles in Δf. The maximum in $\Delta\Gamma$ and the corresponding wiggles in Δf are characteristic of the film resonance. For an explanation of the film resonance, see the third paragraph in Section 2. There is a slight caveat: when a film grows in thickness, the film resonance is expected to occur on the high overtones first because these have the shorter wavelength. The sequence is reversed in Figure 7. The 15 MHz overtone (black) goes into the resonance first. Such a scenario can be explained in a few different ways, but these explanations modify the simple description in terms of the film resonance.

An optical image of the sample from Figure 7A taken after the experiment is shown in **Figure 9**A. The images in Figure 9B,C are shown for comparison. These are thick deposits. In Figure 9B,

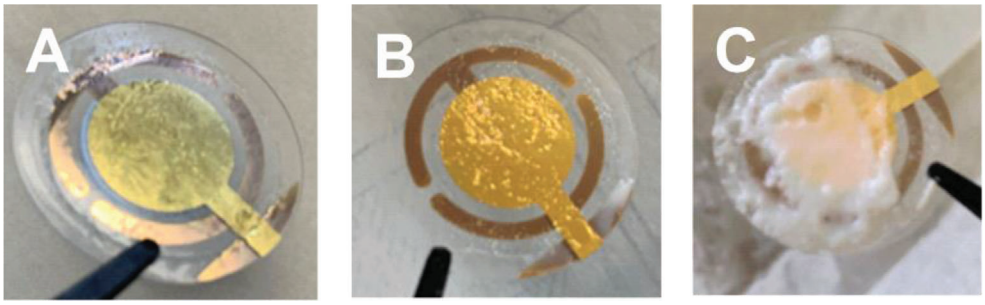

Figure 9. Images taken ex situ from resonators after the experiments: A) from Figure 7A (thin film, PBA with acrylic acid), B) from Figure 5A (thick PBA deposit, incomplete coverage), C) from Figure 5E (thick PMMA deposit, complete coverage).

the clumps of fowling material do not cover the entire surface. In Figure 9C, the entire surface is covered. In the latter case, the shifts of frequency and bandwidth may be evaluated to derive the sample's shear modulus (Section S IV, Supporting Information).

Arguably, the thin layer from Figure 9A should not even be called a fouling layer, but rather a passivation layer. A passivation of this kind is well-known, sometimes referred to as "blocking"[12,38] (not be confused with the blocking of narrow pores in membrane fouling). Because particles in the bulk repel each other as long as the dispersion is colloidally stable, a thin layer of particles also repels particles from the bulk, thereby stopping the fouling process. This scenario is also known in bioengineering as a strategy to avoid the accumulation of thick protein layers at a surface.[39] Hypothetically, the layers formed in the experiments reported in Figure 7 may be portrayed as an antifouling layer in this sense.

5.2. Particle Fouling

Figure 10 shows data acquired with temperature ramps. The gray lines on the left are the nominal temperature. The right-hand side displays the data from the left versus nominal temperature. There was a substantial amount of fouling in the experiments displayed at the top, whereas fouling was absent in the experiment at the bottom. The latter experiment was carried out on a dispersion containing acrylic acid added for stabilization.

We undertook many experiments of this kind. For technical dispersions, particle fouling in temperature ramps was the exception. What is displayed at the bottom in Figure 10 was the rule. This statement applies to hydrophilic as well as hydrophobic surfaces (SiO_x and polystyrene). It also applies to experiments where the electrical potential of the resonator surface was actively controlled and set to various values inside the electrochemical window of water, making use of an electrochemical setup. All these dispersions were colloidally stable in the sense that they did not undergo fouling under any of these conditions.

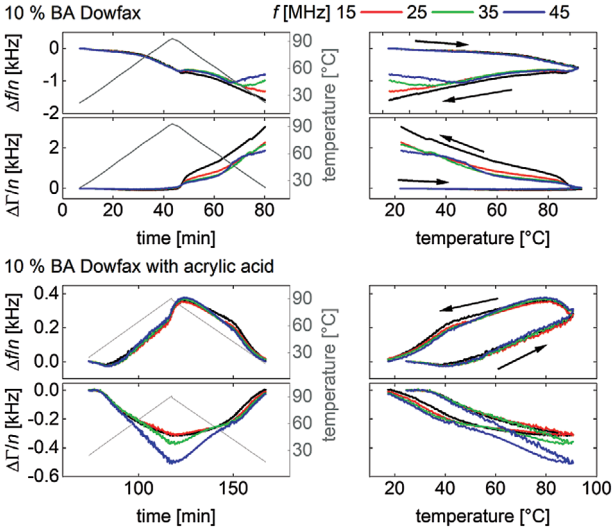

Figure 10. Tests for particle fouling with temperature ramps. The panels on the right contain the same data as the panels on the left, plotted versus nominal temperature. Latexes prepared without acrylic acid do precipitate at high temperature (top), while a latex prepared under similar conditions with added acrylic acid does not (bottom).

6. Conclusions and Outlook

Running a QCM as a heat-transfer surface entails some compromises in precision, but is still perfectly feasible and allows to study heat-transfer fouling in emulsion polymerization. A ring-shaped thermal pad may heat the resonator from the back and still let the damping be tolerable. Experiments at constant temperature gave more robust results than temperature ramps (which are also possible). Two different pathways were observed. In some cases, thick layers formed as evidenced from the relative magnitude of $\Delta\Gamma$ and $-\Delta f$ and, also, from the absence of a film resonance. Optical images taken ex situ after the experiment confirmed this interpretation. Judging from the small increase in $\Delta\Gamma$ occurring a few minutes before the main transition, coagulum forms in the bulk and then attaches to the surface. In other cases, a thin, stable film formed, which passivated the hot surface against further fouling.

A systematic evaluation of parameters, which lead to either of the two pathways, is left for future work. Candidates are colloid stability (improved by the addition of acrylic acid), wettability of the surface, and particle softness (larger for PBA than for PMMA). Potential other factors of influence readily come to mind. This work proves the existence of the different pathways, which is of interest in itself.

Supporting Information

Supporting Information is available from the Wiley Online Library or from the author.

Acknowledgements

Resonators coated with a layer mimicking stainless steel were kindly provided by Ingmar Bialuch, Fraunhofer IST, Braunschweig. Roland Zain (Institute of Organic Chemistry, TUC) constructed the bent glass tube.

Open access funding enabled and organized by Projekt DEAL.

Conflict of Interest

The authors declare no conflict of interest.

Data Availability Statement

The data that support the findings of this study are available from the corresponding author upon reasonable request.

Keywords

emulsion polymerization, heat transfer fouling, polymerization fouling, quartz crystal microbalance (QCM)

Received: October 25, 2021
Revised: December 23, 2021
Published online: January 6, 2022

[1] W. S. Guo, H. H. Ngo, J. X. Li, *Bioresour. Technol.* **2012**, *122*, 27.
[2] N. Epstein, *Heat Transfer Eng.* **1983**, *4*, 43.
[3] R. Steinhagen, H. Müller-Steinhagen, K. Maani, *Heat Transfer Eng.* **1993**, *14*, 19.
[4] D. Q. Kern, R. E. Seaton, *Br. Chem. Eng.* **1959**, *4*, 258.
[5] H. Müller-Steinhagen, *Heat Transfer Eng.* **2011**, *32*, 1.
[6] T. R. Bott, *Fouling of Heat Exchangers*, Elsevier Science, Amsterdam **1995**.
[7] C. S. Chern, Y. C. Chen, *Colloid Polym. Sci.* **1997**, *275*, 124.
[8] J. Urrutia, A. Pena, J. M. Asua, *Macromol. React. Eng.* **2017**, *11*, 1600043.
[9] J. Urrutia, *Ph.D. Thesis*, University of the Basque Country, San Sebastián **2016**.
[10] M. Madani, *Ph.D. Thesis*, University of Hamburg **2021**.
[11] J. Meuldijk, C. J. G. Vanstrien, F. Vandoormalen, D. Thoenes, *Chem. Eng. Sci.* **1992**, *47*, 2603.
[12] C. Henry, J. P. Minier, G. Lefevre, *Adv. Colloid Interface Sci.* **2012**, *185–186*, 34.
[13] A. P. Watkinson, *Chem. Eng. Technol.* **1992**, *15*, 82.
[14] C. B. Panchal, A. P. Watkinson, presented at ASME/AIChE National Heat Transfer Conf., Atlanta, August **1993**.
[15] A. Hohlen, W. Augustin, S. Scholl, *Macromol. React. Eng.* **2020**, *14*, 1900035.
[16] E. Wallhausser, M. A. Hussein, T. Becker, *Food Control* **2012**, *27*, 1.
[17] J. Cen, M. Vukas, G. Barton, J. Kavanagh, H. G. L. Coster, *J. Membr. Sci.* **2015**, *484*, 133.
[18] A. Lasia, *Electrochemical Impedance Spectroscopy and Its Applications*, Springer, Heidelberg **2014**.
[19] J. Wegener, C. R. Keese, I. Giaever, *Exp. Cell Res.* **2000**, *259*, 158.
[20] E. Wallhausser, W. B. Hussein, M. A. Hussein, J. Hinrichs, T. M. Becker, *J. Food Eng.* **2011**, *103*, 449.
[21] A. Pereira, R. Rosmaninho, J. Mendes, L. F. Melo, *Food Bioprod. Process.* **2006**, *84*, 366.
[22] C. Steinem, A. Janshoff, *Piezoeletric Sensors*, Springer, Heidelberg **2007**.
[23] D. Johannsmann, C. Leppin, A. Langhoff, *Sensors* **2021**, *21*, 3490.
[24] T. E. Alexander, L. D. Lozeau, T. A. Camesano, *Cell Surf.* **2019**, *5*, 100024.
[25] T. Kallio, J. Kekkonen, P. Stenius, *J. Adhes.* **2004**, *80*, 933.
[26] Y. Lu, Q. Wei, Y. Cheng, X. D. Ren, H. Wang, J. Xie, *Int. J. Electrochem. Sci.* **2021**, *16*, 21057.
[27] V. Reipa, J. Almeida, K. D. Cole, *J. Microbiol. Methods* **2006**, *66*, 449.
[28] C. Sprung, D. Wahlisch, R. Huttl, J. Seidel, A. Meyer, G. Wolf, *Water Sci. Technol.* **2009**, *59*, 543.
[29] D. E. Delgado, L. F. Sturdy, C. W. Burkhart, K. R. Shull, *J. Polym. Sci., Part B: Polym. Phys.* **2019**, *57*, 1246.
[30] R. Groves, H. K. Tong, Y. M. Chong, K. C. Fong, in *A Technique to Study the Early Stages of the Coagulant Dipping Process*, 5th IRGC, Malaysian Rubber Glove Manufacturers' Association (MARGMA), Petaling Jaya, Malaysia **2010**.
[31] M. Heinisch, E. K. Reichel, I. Dufour, B. Jakoby, *Sens. Actuators, A* **2007**, *186*, 111.
[32] P. Sievers, C. Moß, U. Schröder, D. Johannsmann, *Biosens. Bioelectron.* **2018**, *110*, 225.
[33] K. K. Kanazawa, J. G. Gordon, *Anal. Chem.* **1985**, *57*, 1770.
[34] K. R. Shull, M. Taghon, Q. F. Wang, *Biointerphases* **2020**, *15*, 12.
[35] Makarov Instruments, https://www.makarov.ca/vna.htm (accessed: May 2021).
[36] A. F. Routh, W. B. Russel, *Ind. Eng. Chem. Res.* **2001**, *40*, 4302.
[37] G. Sauerbrey, *Z. Phys.* **1959**, *155*, 206.
[38] B. Vincent, C. A. Young, T. F. Tadros, *Faraday Discuss.* **1978**, *65*, 296.
[39] B. D. Ratner, in *Biomaterials Science*, (Eds: B. D. Ratner, A. S. Hoffmann, F. J. Schoen, J. E. Lemons), Elsevier, Amsterdam **2012**, section I.2.10.

